THz BENCH TESTS OF A SLAB-SYMMETRIC DIELECTRIC WAVEGUIDE*

F. Lemery[1], H. Panuganti[1], D. Mihalcea[2], P. Piot[1,2], P. Stoltz[3]
[1] Department of Physics and Northern Illinois Center for Accelerator & Detector Development, Northern Illinois University DeKalb, IL 60115, USA
[2] Accelerator Physics Center, Fermi National Accelerator Laboratory, Batavia, IL 60510, USA
[3] Tech-X Corporation, Boulder, CO 80303, USA

Abstract

Dielectric-lined waveguides (DLW) are gaining popularity for beam driven acceleration applications. An experiment to demonstrate beam-driven acceleration using a slab-symmetric dielectric-lined waveguide driven by a flat beam is in preparation at the Advanced Superconducting Test Accelerator (ASTA) at Fermilab. In this paper we detail an on-going experiment aimed at characterizing the structure using a THz pulse obtained from optical rectification. After propagation through the DLW structure, the THz pulse is analyzed using a Michelson interferometer and eventually a single-shot electro-optical imaging.

INTRODUCTION

Dielectric wakefield acceleration in dielectric-lined waveguides (DLW's) presents an attractive alternative to conventional accelerators due to its relative low cost and capability to sustain higher acceleration gradients. One way of powering these DLW structures is to excite an electromagnetic wake by propagating a high-charge "drive" bunch [1, 2]. A properly delayed "witness" bunch can then experience a net acceleration. Alternatively, DLW structures can be powered by lasers [3, 4].

To date, cylindrically-symmetric DLW's have been extensively studied both theoretically and experimentally [5]. At low energy these type of structures put stringent requirement on the drive-beam emittance [6] and an asymmetric slab structure combined with a flat beam – a beam with high transverse emittance ratio – can alleviate these requirements [7, 8]. In the latter configuration, the beam passes between two flat dielectric slabs having their outer surfaces metallized; see Fig. 1(a). For a given gap (radius) size and drive-bunch parameters, the slab geometry generally provide a weaker wakefield than its cylindrical-symmetric counterpart.

In slab DLW's the electromagnetic modes can be categorized into two types [9] longitudinal section electric (LSE) and longitudinal section magnetic (LSM) corresponding respectively to the boundary conditions $E_y = 0$ and $H_y = 0$ at the vacuum-dielectric interface (the axis configuration is shown in Fig. 3. The lowest-order LSM mode is typically used for producing the axial electric field E_z necessary for acceleration. Figure 2 presents the dispersion curve $k(\omega)$ associated to the LSM modes.

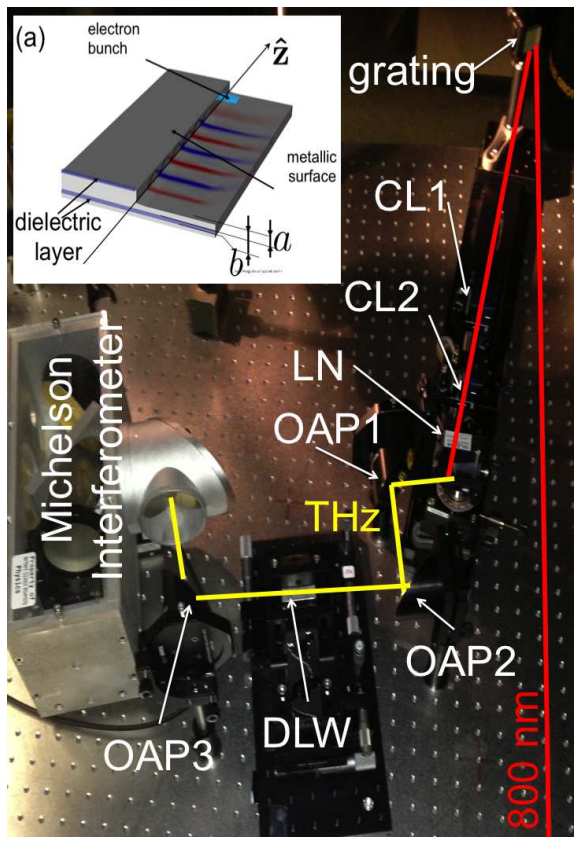

Figure 1: Experimental setup used to characterize DLW structures (photograph) and geometry of the DLW under consideration (inset schematic). The legend is as follows "CL", "OAP" and "LN" respectively stand for "cylindrical lens", "off-axis parabolic mirror", and "$LiNbO_3$ crystal". The red lines indicate the path of the 800-nm 4-mJ IR pulse and the yellow lines correspond to the THz beam.

In preparation for an experiment at the Advanced Superconducting Test Accelerator (ASTA) at Fermilab we are developing a THz bench test for slab DLWs. In this setup a THz pulse is used to probe the electromagnetic properties of the slab DLW using a near-field THz mapping technique similar to what was developed in Ref. [10]. The method can be used to obtained spatial distributions of the modes

* This work was supported by the DTRA award # HDTRA1-10-1-0051 to Northern Illinois University.

Copyright © 2013 by JACoW — cc Creative Commons Attribution 3.0 (CC-BY-3.0)

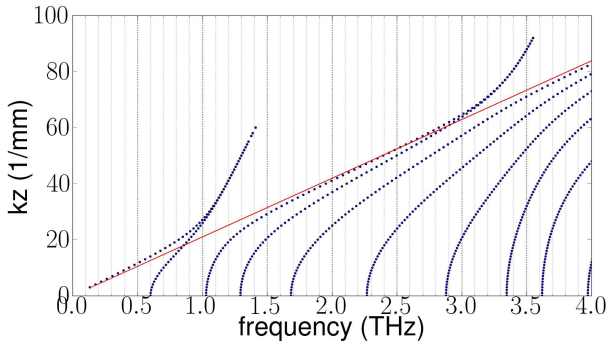

Figure 2: Dispersion relation associated to the LSM modes in a slab-symmetric DLW with parameter $a = 100\ \mu m$ and $b = 120\ \mu m$. The red line correspond to $k_z = 2\pi f c$.

along with their dispersion relations.

EXPERIMENTAL SETUP

The experimental setup to be used to characterize the DLW's is depicted in Fig. 1. The basic idea is to eventually perform a near-field mapping of a guided short THz pulse at the input and the output of the DLW.

A 4-mJ, 800-nm amplified laser pulse produced by a commercial laser system is used to produce a THz pulse. The laser is obtained from regenerative amplification of a broadband $\delta\lambda \simeq 100$ nm pulse. Several method to produced THz were attempted: "conventional" optical rectification by impinging a ZnTe crystal with 100 cut and phase-matched optical rectification using a $LiNbO_3$ (LN) wedged crystal [11, 12]. Because of its significantly higher yield and relatively easy implementation we choose the latter method as shown in Fig. 1 and use a stoichiometric MgO(0.6%):LiNBO3 crystal with a 5×5 mm^2 entrance-face size.

The pulse impinges a 1200-lines/mm grating to provide the necessary wavefront tilt. A cylindrical lens focusing in the horizontal plane (CL1, $f = 15$ cm) provides an approximate image of the grating onto the LN crystal. A second cylindrical lens (CL2) is used to focus the beam vertically. The typical spot on the LN crystal face is $w_x \times w_y \simeq 3 \times 0.5$ mm^2. Upon exiting the LN crystal, the THz beam is collimated with an off-axis parabolic mirror (OAP1) and focused inside the DLW structure (OAP2). The transmitted THz beam is then collimated (using OAP3 and 4) and sent to a Michelson interferometer equipped with a Helium-cooled InSb bolometer. In a later stage we plan to have an electro-optical imaging diagnostics.

SIMULATION AND ANALYSIS OF A THZ PULSE PROPAGATION IN A SLAB DLW

To assess the performance of the described experimental setup we modeled the propagation of a THz pulse through the DLW and use these numerical results to develop analysis tools. The simulation of a THz pulse through the DLW were performed using the program VORPAL [13]. VORPAL uses the conformal finite difference time domain (CFDTD) method to solve Maxwell's equations. The geometry of the problem simulated with VORPAL appears in Fig. 3.

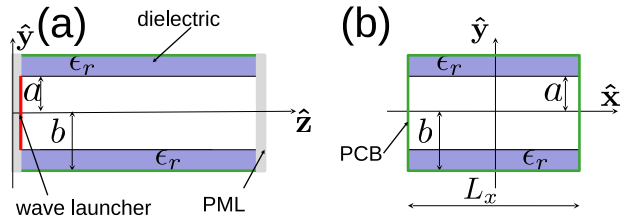

Figure 3: A diagram of the slab from the x-transverse direction (a) and the from the z-longitdinal direction (b). The slab is composed of a dielectric coating with dielectric permitivity ϵ_r surrounded by a perfectly conductive boundary (PCB). In the VORPAL simulation, we inject the THz pulse using a current $\vec{J}$ to drive a short pulse in z. Lastly, to remove reflections and to artificially produce the pulse leaving the structure we implement a perfectly matched layer (PML). We record the signal on axis, near the PML.

For the results presented below, a THz pulse is launched from the $(x = 0, y, z)$ plane using a time dependent current density

$$\vec{J}_z(t) = A_0 t \sin(\omega_1 t)\sin(\omega_2 t)\sin(\omega_3 t)e^{-(t-t_0)^2/(\tau^2)}, \quad (1)$$

where $\omega_i \equiv 2\pi f_i$ where $(f_1, f_2, f_3) = (0.8, 1.0, 1.2)$ THz, $t_0 = 2$ ps, and the full-width half-max (FWHM) duration is $\tau = 1$ ps. Although the pulse peaks at frequencies f_i, its relatively large bandwidth $\delta f \simeq \tau^{-1} \simeq 1$ THz allows for the excitation of higher frequencies modes. The electromagnetic field of the guided pulse are recorded on a two-dimensional grid-line as a function of time at the entrance $E_u(x, y = 80\ \mu m, z = 0, t)$ and at the exit $E_u(x, y = 80\ \mu\text{m}, z = 2\ \text{cm}, t)$ (where $u \in [x, y, z]$ corresponds to the three field components).

The Fourier transform of the pulse before and after propagating through the structure provides a partial understanding of the propagation of the modes through the structure. The surviving frequencies correspond to the eigenmodes of the structure while components which have faded can be associated to the evanescent modes. Figure 4 shows the Fourier transform of the E_y component at the entrance and exit of the DLW structure. The spatial variations of the frequency content within the pulses is indicative of the mode's spatial distributions.

We import the signal recorded at the end of the structure into another program for spatio-temporal analysis. For each grid point recorded on the transverse line at the exit of the structure, we use a moving window to scan through the signal temporally. At each window step, we perform a Fourier transform and record the strength of the Fourier component of a selected frequency. To reduce any unwanted artifacts, e.g., from sharp edges the moving win-

Copyright © 2013 by JACoW — cc Creative Commons Attribution 3.0 (CC-BY-3.0)

ISBN 978-3-95450-122-9

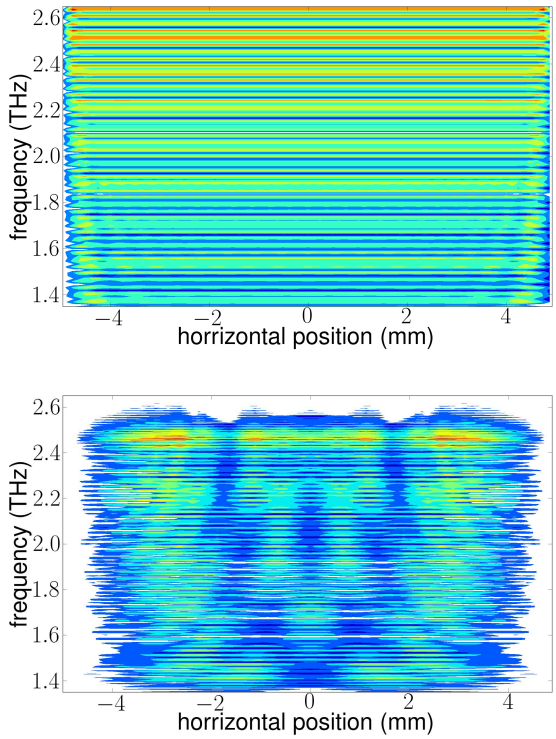

Figure 4: Fourier transform of the pulse at the entrance of the structure $|E_y(x = 0, y = 80\ \mu m, z = 0, f)|$ (top) and a Fourier transform of the pulse at the end of the structure$|E_y(x = 0, y = 80\ \mu m, z = 2\ cm, f)|$ (bottom).

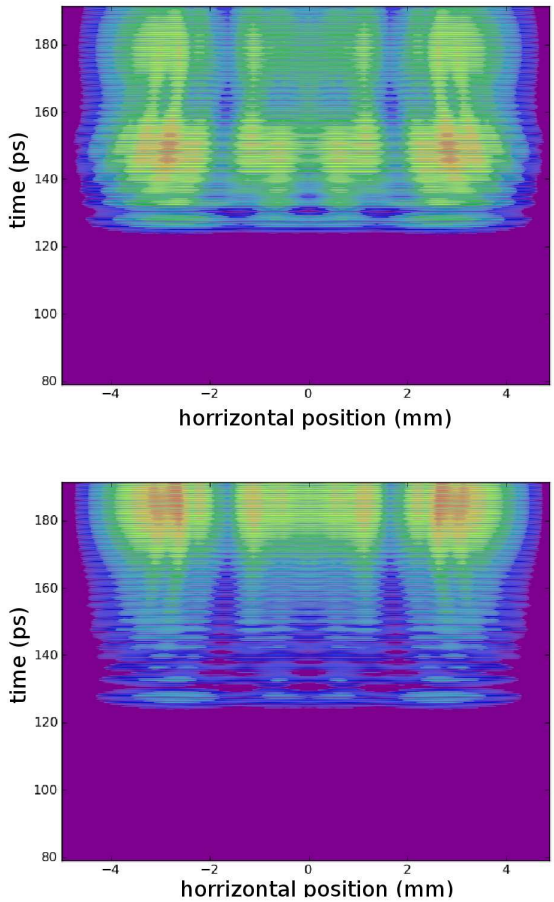

Figure 5: Spatio-temporal distribution of the guided pulse (shown in Fig. 4) filtered at 1.4 THz (top) and 1.6 THz (bottom).

dows is a Hann window

$$w(n) = 0.5\ \left[1 - \cos\left(\frac{2\pi n}{N-1}\right)\right], \qquad (2)$$

for an individual point n, of N sampled points.

In Fig. 5 we show the spatio-temporal distribution of the guided pulse associated to the filtered frequencies of 1.4 and 1.6 THz. Using this method, and comparing to the dispersion curve above, we can confirm the propagation of the LSM_{2m} and LSM_{3m} for the 1.4 THz component as well as the propagation of the LSM_{2m}, LSM_{3m} and the near cutoff region of the LSM_{4m} (which explains its tardiness passing through the structure) for the 1.6 THz component. In addition to providing information on the modes' spatial distribution, the technique can also be used to deduce the group velocity of the modes.

STATUS AND CONCLUSION

An experimental setup to support the characterization of DLW structure was assembled and first results on the THz pulse production were recently measured. In this paper we presented numerical simulation to benchmark our analysis technique. Our results shows that quantitive information on the DLW mode can be obtained. The experiment is being carried used the laser available at the high brightness electron source laboratory (HBESL) at Fermilab National Accelerator Laboratory.

REFERENCES

[1] C. T. M. Chang, *et al.*, **41**, 4493 (1970).
[2] M. Rosing *et al.*, Phys. Rev. D **42**, 1829 (1990).
[3] G. Travish, AIP Conf. Proc. **1507**, 85 (2013).
[4] L. Wong, *et al.*, Opt. Exp. **21** (8), 9792 (2013).
[5] W. Gai, *et al.*, Phys. Rev. Lett. **61**, 2756 (1988).
[6] F. Lemery, *et al.*, these proceedings.
[7] A. Tremaine *et al.*, Phys. Rev. E **56**, 7204 (1997).
[8] D. Mihalcea, *et al.*, Phys. Rev. STAB **15**, 081304 (2012).
[9] J.T. Bernhard and W.T. Joines, Journal of Microwave Power and Electromagnetic Energy, **30**, 2 (1995).
[10] O. Mitrofanov, *et al.*, Appl. Phys. Lett. **94**, 171104 (2009).
[11] J. Hebling, *et al.*, Opt. Exp. **21**, 1161 (2002).
[12] J. A. Fülöp, *et al.*, Opt. Lett. **37**, 4 (2012).
[13] C. Nieter, J. R. Cary, J. Comp. Phys. **169**, 448 (2008).

Copyright © 2013 by JACoW — cc Creative Commons Attribution 3.0 (CC-BY-3.0)